Solar Energy Materials and Solar Cells 172 (2017) 1–10

Contents lists available at ScienceDirect

Solar Energy Materials and Solar Cells

journal homepage: www.elsevier.com/locate/solmat

# P3HT as a pinhole blocking back contact for CdTe thin film solar cells

J.D. Major[a,*], L.J. Phillips[a], M. Al Turkestani[b], L. Bowen[c], T.J. Whittles[a], V.R. Dhanak[a], K. Durose[a]

[a] Stephenson Institute for Renewable Energy and Department of Physics, University of Liverpool, Liverpool L69 7ZF, UK
[b] Department of Physics, Umm Al-Qura University, Al Jamiah, 7549, Mecca 24243, Saudi Arabia
[c] G. J. Russell Microscopy Facility, Durham University, South Road, Durham DH1 3LE, UK

ARTICLE INFO

*Keywords:*
Photovoltaics
Cadmium telluride
Contacts
Organic

ABSTRACT

A new approach to back contacting CdTe solar cells that uses an organic poly(3-hexythiophene-2,5-diyl) (P3HT) back contact layer is reported. The most striking benefit of P3HT was demonstrated to be through a "pinhole blocking" effect, significantly improving performance uniformity. This was demonstrated through comparison of open circuit voltage values for a large sample set (600 cells) and through measurement of a device with a graded absorber layer thickness (0.7–1.9 μm). The conversion efficiency achievable and the electrical barrier height of the contacts to the CdTe were also investigated for P3HT/Au and Au control contacts – both being tested with and without additional Cu. Temperature dependent *JV* measurement showed the use of P3HT reduced the barrier to (0.29–0.33 eV) from the value achievable with Au (0.39–0.42 eV), but inclusion of Cu into either of the structures gave the lowest barriers (0.21–0.22 eV). For the data sets recorded, P3HT/Au yielded higher peak efficiencies than the Au control contact. However, when Cu was included the peak performance of devices having P3HT/Cu/Au and Cu/Au contacts were comparable at 14.7% respectively but the P3HT/Cu/Au contact displayed a significantly higher average performance through increased uniformity of the device response.

## 1. Introduction

Establishing an Ohmic back contact for CdTe thin film solar cells is a fundamental issue of the material and is one of the primary process challenges of cell fabrication. Owing to the high electron affinity of CdTe, a metal with a work function in excess of ~ 6 eV is required to yield an Ohmic contact to p-type CdTe. As a result direct contact with standard metals such as nickel, aluminium or gold, results in the formation of a back contact barrier [1]. This generates a diode which opposes the main junction diode and causes the commonly observed phenomenon of 'rollover' in current-voltage (*JV*) curves for CdTe solar cells [2,3]. At high forward bias the current response is limited and the degree of rollover observed is related to the height of the back contact barrier [1]. For significantly large barriers, cell performance becomes compromised by a reduced fill factor (*FF*) [3]. To account for this issue the typical solution is to incorporate Cu into the CdTe back surface via the formation a CuTe layer [4], that acts to dope the surface highly p-type. Whilst undoubtedly a successful technique the issue remains that since Cu is a faster diffuser in CdTe its inclusion can reduce long term cell stability and subsequent performance loss. Cells which include Cu in the back contact have been shown to suffer from long term stability issue [5], although this can be accounted for, to an extent, through the use of very thin Cu films, < 5 nm, or through the additional inclusion of back contact buffer layers such as ZnTe [6] or $Sb_2Te_3$ [7]. The fundamental electrical barrier and the known stability issues associated with Cu have led to a large number of alternative contact processes for CdTe being investigated. Work has been reported utilising pyrite [8] or high work function transition metal oxides such as $MoO_x$ [9–11]. Back contact research for CdTe has thus far focussed mainly on the use of inorganic materials. This neglects a significant opportunity that exists through the use of organic layers such as P3HT (poly(3-hexythiophene-2,5-diyl)) and hole transporting materials such as PEDOT:PSS (poly (3,4-ethylenedioxythiophene) polystyrene sulfonate) or SPIRO OMeTAD ($N^2$,$N^2$,$N^{2'}$,$N^{2'}$,$N^7$,$N^7$,$N^{7'}$,$N^{7'}$-octakis(4-methoxyphenyl)-9,9′-spirobi [9H-fluorene]-2,2′,7,7′-tetramine) for example. Thus far only PEDOT:PSS has been properly investigated for thin film CdTe devices [12]. Whilst it's incorporation showed an improvement in comparison to simple gold contacts, the devices showed a large (> 3%) reduction in efficiency compared to those having optimised Cu/Au contacts. Amongst the range of organic compounds that may be considered P3HT is a promising candidate. Whilst it is typically considered as a absorber layer rather than a hole transporting layer, the expected positions of its valence and conduction bands relative to CdTe should aid hole extraction at the back contact whilst also providing a barrier to electron transport in the conduction band. As well as being widely used in organic PV and hybrid perovskites, it has also shown promise in CdTe

* Corresponding author.
*E-mail address:* jon.major@liverpool.ac.uk (J.D. Major).

http://dx.doi.org/10.1016/j.solmat.2017.07.005
Received 25 April 2017; Received in revised form 6 July 2017; Accepted 9 July 2017

bulk heterojunction devices [13], CdTe–ZnO nanocomposite devices [14] or when prepared as a nanocrystal and combined with CdTe nanocrystals [15].

A less widely studied issue for polycrystalline CdTe solar cells is the phenomenon of non-uniformity and shunting, or pinhole, related performance losses. Due to variations in the grain structure, arising from factors such as the choice of deposition conditions, contamination on the surface prior to deposition or scratches during post deposition processing, either partial or full physical shunting pathways may be formed in the CdTe layer which degrade device performance [16]. These may take the form of a complete pinhole in which case the metallic back contact completely penetrates the CdTe layer and the cell short circuits. More commonly though there are incomplete pinholes or other defects that act as "weak diodes" leading to losses in $V_{oc}$ and *FF* [17–20]. Previously routes to correct for weak diode or pinhole regions have focussed on the use of spatially selective electrochemical polymerization methods to deposit resistive polymer films such as polyaniline [21,22] or pyrrole [23]. In these techniques the cell is biased via the front contact and, due to surface potential being higher at weak diode regions, deposition of the polymer occurs primarily at weak diode positions. This paper reports a different approach wherein P3HT is directly deposited from solution via spin coating and unlike the electrochemical techniques is able to act as a dual back contact and pinhole blocking layer. In this work P3HT-containing contact structures were investigated on CdTe devices that had been intentionally grown with protocols that encouraged poor device uniformity. CdTe solar cells contacted with P3HT are shown to have improved average and peak performances and reduced rollover in comparison to Au contacted solar cells. Importantly they have improved performance uniformity over that of Cu/Au contacted devices while maintaining comparable peak efficiencies.

## 2. Experimental section

### 2.1. Cell fabrication

CdTe cells were deposited on $SnO_2$:F (FTO) TEC6 glass from NSG ltd. RF sputtering was used to deposit ~ 100 nm ZnO films as a buffer layer at room temperature, followed by ~ 160 nm of CdS at 200 °C both using a 5 mTorr argon plasma. For devices which incorporated a CdS:O layer no ZnO buffer layer was used and CdS:O films were sputtered at room temperature at 5 mTorr with a 7% oxygen in argon gas mixture. CdTe was deposited via close space sublimation (CSS) using source and substrate temperatures of 605 °C and 520 °C and a nitrogen ambient of 25 Torr. Post-growth the samples were etched for 15 s in a nitric-phosphoric (NP) acid solution [24] prior to deposition of $MgCl_2$ [25] onto the sample back surface using spray deposition from a 1 Molar solution in water (Alfa Aesar). Annealing was done in a tube furnace under an air ambient at a temperature of 420 °C for 25 min. Post-annealing the samples were rinsed with DI water before being NP etched for a further 15 s prior to back contacting. All samples utilised a grid of 0.25 $cm^2$ gold back contacts which were deposited by thermal evaporation at room temperature.

### 2.2. Contacting

P3HT was prepared by dissolving 15 mg poly(3-hexythiophene-2,5-diyl) (Sigma Aldrich, average Mn 54,000–75,000, 99.995%) in 1 ml of chlorobenzene (Sigma Aldrich, anhydrous, 99.8%). The solution is gently heated to 70 °C with stirring for 1hr to complete dissolution. Once cooled, the solution is filtered with a 0.22 μm PTFE filter before use. The P3HT solution was deposited onto the CdTe surface via spin coating at in the range 500–4000 rpm and with durations of 10–60 s. Where copper was included in the back contact this was deposited as an ~ 5 nm layer via thermal evaporation at room temperature either before or after P3HT deposition. Annealing of contact structures was done on a hotplate in an air ambient at 150 °C.

### 2.3. Characterisation

Current voltage (*JV*) analysis was performed using a TS Space Systems solar simulator calibrated with a GaAs reference cell to the AM1.5 spectrum intensity. For *JV* measurements performed as a function of temperature (JVT) a CTI-cryogenics cryostat over a temperature range of 200–300 K with *JV* measurements recorded via a Keithley 2400 sourcemeter. External quantum efficiency (EQE) measurements used a Bentham PVE3000 analysis system. SEM images were recorded using a Hitachi SU-70 microscope in secondary electron mode whilst optical microscope images used was a Nikon Eclipse LV100.

The ionisation potential was determined positions by XPS using a SPECS monochromatic Al Kα X-ray source ($h\nu$ = 1486.6 eV) in conjunction with a PSP Vacuum Technology electron-energy analyser. Further details of the system and the measurement procedure are detailed elsewhere [26]. Samples were measured before and after in vacuo cleaning which consisted of 500 eV $Ar^+$ ion bombardment for 5 min in order to remove the layer of contamination inevitably present on the surface of the samples.

## 3. Results and discussion

### 3.1. P3HT coating quality and band positions

Consistent and uniform coatings of P3HT onto close space sublimation (CSS) deposited CdTe could be achieved using a spin speed of 4000 rpm for a duration 30 s using a 100 μl solution volume deposited in a single step. Experimentally it was found that the usual variables in spin coating affected the quality of the deposit, including the smoothness of the CdTe – sputtered CdTe is considerably smoother than CSS-grown CdTe. However these conditions were found to be effective in most cases.

Fig. 1a–d show comparisons of the uncoated and coated CdTe surfaces examined by both light and SEM microscopy. While the light microscopy demonstrated that the P3HT coated the CdTe uniformly on a macroscopic scale, the SEM showed that the rough granular structure of the CdTe was coated conformally by the organic material. The original grain structure of the CdTe is clearly visible beneath the P3HT layer, and there is no evidence of gaps in the coverage. This is confirmed by the SEM image of the focussed ion beam milled cross section [27] shown in Fig. 1e. The P3HT is < 50 nm thick away from grain boundary positions and it provides complete coverage. Moreover it may be seen to infill crevasses at the grain boundary positions while simultaneously covering the high points on the surface. Uncoated samples have numerous complete pinholes that are visible to the naked eye as bright spots when the sample is backlit. Following P3HT deposition such pinholes are no longer visible. These physical observations are consistent with the evidence for electrical pinhole blocking by the P3HT presented later.

In order to investigate the inevitable contact/CdTe electrical barrier, X-ray photoelectron spectroscopy (XPS) was used to assess the valence band positions of P3HT with respect to CdTe via measurement of the ionisation potential (IP) [26]. Fig. 2a shows the secondary electron cutoff (SEC) and valence band maximum (VBM) data from XPS measurements of complete cell structures for i) the uncoated CdTe surface, ii) as-deposited P3HT on the same CdTe surface and iii) P3HT following an air annealing. The comparison of as-deposited with air-annealed P3HT was included since devices made using them showed significant differences in their forward current roll over as shown in *JV* curves in Fig. 3. It was therefore suspected that annealing causes a change in the contact band alignment.

Values for the IP for both CdTe and P3HT are shown in the inset panel of Fig. 2. The table shows data for both the as-deposited surfaces and that for surfaces that have undergone an in-UHV sputter-clean

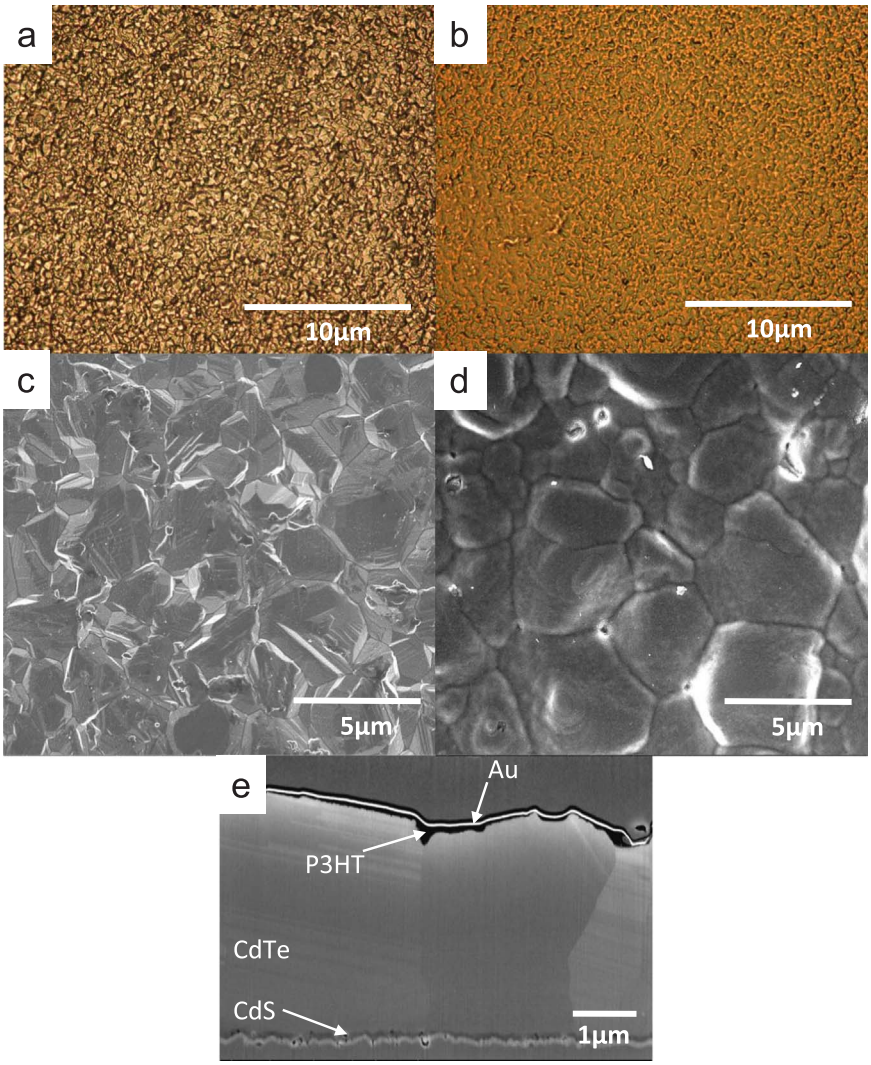


**Fig. 1.** Microscopy analysis of device structures showing of the back surface for CdTe and P3HT coated CdTe, using optical microscopy, a) and b) respectively, and SEM, c) and d) respectively. Figure e) shows a focus ion beam milled device cross section of a P3HT coated gold contacted device.

process to remove the uppermost ~ 1 nm from the surfaces. Since XPS is highly surface sensitive this comparison was essential to eliminate unwanted contributions from surface phases. In the case of CdTe, cleaning increased the measured IP from 4.90 eV to a value of 6.07 eV. This value is higher than for theoretical predictions [28,29] or for single crystal measurements, such as the IP of 5.69 eV measured by Teeter et al. [30] for example. However both the theoretical predictions and single crystal work do not account for the influence of the chloride treatment, which may have a significant influence. In comparison cleaning P3HT acted to reduce the observed IP – from 5.41eV to 5.08 eV for as-deposited and 6.36 eV to 5.03eV for air-annealed samples. Indeed the values for both cleaned P3HT sample types were comparable, giving confidence in the method. The IP values of the cleaned CdTe and P3HT samples are used to show relative band positions with Au in Fig. 2c. This can only offer a guide to the 'natural band alignment' using aligned vacuum levels rather than a true band alignment which requires measured interface offsets. The band positions shows some features that confirm that P3HT may be a good contact for CdTe: Firstly, there is a barrier-free pathway for holes to leave the p-CdTe, as is required for a back contact. Secondly, the band positions provide a step in the conduction band that acts as a barrier to minority carrier electrons that are moving contrary to the expected current flow direction. Such electron-reflecting barriers are well known in silicon PV device technology and have been postulated as desirable structures for CdTe PV devices [31,32]. Finally we acknowledge that since this predicted band scheme is based on the IP data for cleaned samples, and no such UHV cleaning is used in practice, real devices may behave differently from as-predicted due to surface contamination.

### 3.2. P3HT contacting comparison

An initial assessment of the impact of P3HT on the back contact behaviour was made by comparing cells having three different volumes of P3HT deposited with a control having a simple Au contact. (These experiments were for contacts having no intentional Cu – see the later section for experiments with Cu). Determination of an appropriate deposition volume is vital to produce a uniform coverage, too small a deposition volume produces poor edge coverage (P3HT is deposited in the centre of the sample and span out), too great a volume leads to areas of P3HT accumulation on the surface and again non-uniform coverage. The P3HT films were prepared by spinning 100, 150 and 200 µl of P3HT solution. For each sample series, a single 50 × 50 $mm^2$ solar cell sample plate was broken into four 25 × 25 $mm^2$ quarters for the comparison. Three were coated with P3HT prior to all four being contacted with grids of nine 0.24 $cm^2$ gold electrodes. The P3HT coated samples were annealed in air at 150 °C for 20 min, as this was found to improve the performance of the contact (*JV* curves before and after annealing are shown in Fig. 3). Gold only contacted cells were not annealed as this was found to degrade them (contrary to the case for P3HT). *JV* analysis was used to compare the device performance of each quarter with average and peak cell performance data given in Table 1. *JV* curves for highest efficiency contacts from each cell quarter are

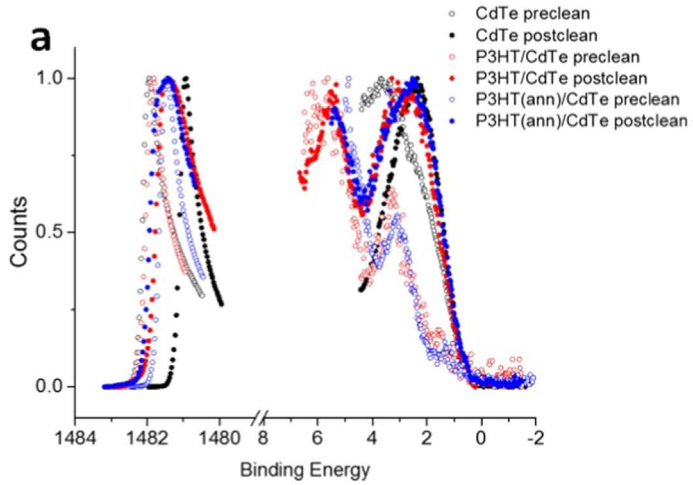


b

| Sample (* is after cleaning) | IP (eV) |
|---|---|
| CdTe | 4.90 |
| CdTe* | 6.07 |
| P3HT/CdTe | 5.41 |
| P3HT/CdTe* | 5.08 |
| P3HT(ann)/CdTe | 6.36 |
| P3HT(ann)/CdTe* | 5.03 |

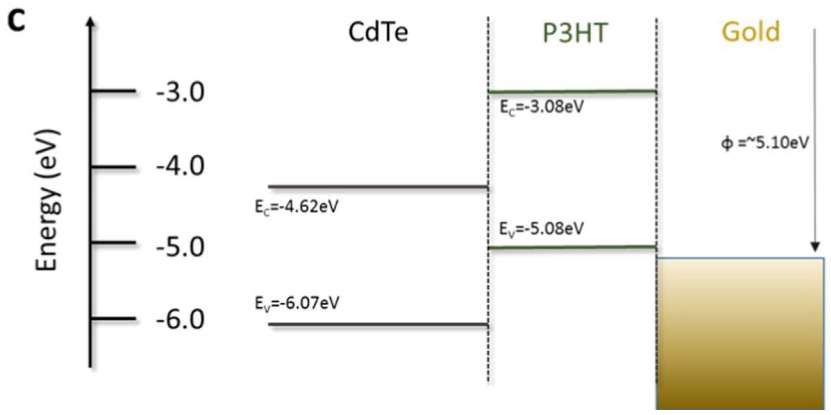


**Fig. 2.** a) XPS spectra of CdTe, P3HT and air annealed P3HT films, b) extracted values for ionisation potential from XPS spectra with and without surface cleaning and c) determined band positions for CdTe P3HT and gold layers following XPS analysis.

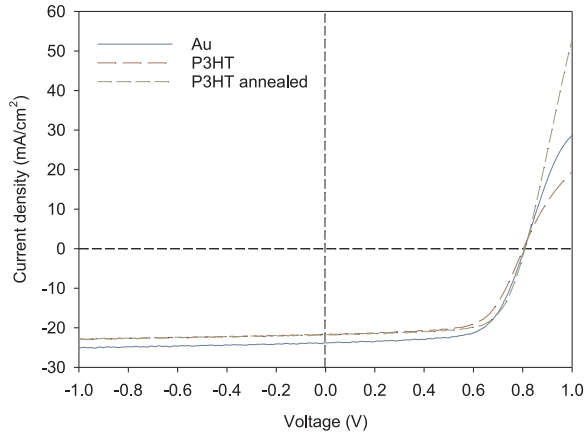


**Fig. 3.** Comparison of the AM1.5 JV curves for CdTe for devices having Au and P3HT/Au contacts. For the P3HT–containing contacts it may be seen that air annealing has acted to reduce the degree of forward bias current roll-over. The cause of this behaviour was explored by investigating the band line ups of the CdTe with P3HT.

given in Fig. 4a.

Addition of P3HT to the back surface was found to improve both the average and peak performance for all volumes of P3HT applied in comparison to a simple Au contact. Although the peak efficiency improvement is only 0.99% for a 100 µl deposition, there is an increase of around 12 mV in the device $V_{oc}$ and from the *JV* curves at high forward bias it is further apparent that rollover has been reduced by the addition of the P3HT layer to the contact structure.

A simple measure of the degree of forward bias current rollover for a *JV* curve is the resistance ratio $R_{1v}/R_{Voc}$ (i.e. the ratio of the resistance at $V = Voc$ to that at 1 V). For devices where rollover is deleterious, this value will be > 1, whereas for cells with an effective back contact $R_{1v}/R_{Voc} < 1$. From the *JV* data in Fig. 4 this value is 1.70 for the Au contacted device falling to 1.04, 0.74 and 0.50 for cells contacted with 100, 150 and 200 µl of P3HT respectively. This confirms that the addition of P3HT was capable of decreasing rollover, and hence the barrier present at the back contact, in comparison to a simple gold back contact. Equally it appeared that while the larger volume 200 µl P3HT deposition produced a slightly improved back contact compared to 100 µl the overall performance was lower, possibly due to the P3HT solution being more resistive than ideal, hence 100 µl was chosen as a standard deposition volume.

It is well established that the primary contacting route to CdTe solar cells is not a simple metallic contact but rather involves the in-diffusion of Cu into the device back surface or else into an intermediary layer such as ZnTe [25]. Hence it is of greater interest not only to compare the behaviour of these P3HT contact layers to Cu/metal contacted devices, but also to explore the possibility of combining P3HT with Cu for contacting. Device results for contact structures with Cu compared to Cu-free controls are shown in Table 2.

Prior to making the sample set reported here, fabrication trials revealed that P3HT layers are essentially “transparent” to Cu i.e. there was no discernible difference in device performance between deposition of Cu before or after the P3HT layer. Hence for processing convenience, a deposition sequence of P3HT deposition by spin coating (100 µl) followed by thermal evaporation of ~ 5 nm Cu and then evaporation of the Au back contacts was established. Cells with P3HT and/or Cu were then annealed for 20 min at 150 °C in air – this time was optimised in trials. The annealing was omitted for cells with Au only

**Table 1**
Contacts without Cu. Cell performance parameters for cells contacted with three thicknesses of P3HT in comparison to an Au-contacted control. In each case the data is for nine unscribed electrodes having an area of 0.24 $cm^2$ each.

| Contact | | Efficiency (%) | $V_{OC}$ (V) | $J_{SC}$ (mA/$cm^2$) | *FF* (%) |
|---|---|---|---|---|---|
| **Au** | *Ave* | 6.32 ± 2.94 | 0.614 ± 0.17 | 20.17 ± 1.23 | 47.65 ± 11.88 |
| | *Peak* | 10.45 | 0.755 | 21.51 | 64.34 |
| **100 µl P3HT** | *Ave* | 10.34 ± 1.01 | 0.748 ± 0.019 | 21.34 ± 0.83 | 64.52 ± 2.64 |
| | *Peak* | 11.54 | 0.767 | 22.79 | 65.74 |
| **150 µl P3HT** | *Ave* | 6.86 ± 4.15 | 0.583 ± 0.26 | 19.82 ± 2.03 | 50.57 ± 16.57 |
| | *Peak* | 11.15 | 0.766 | 21.45 | 67.60 |
| **200 µl P3HT** | *Ave* | 9.56 ± 0.78 | 0.771 ± 0.012 | 19.71 ± 1.01 | 62.86 ± 2.85 |
| | *Peak* | 10.69 | 0.752 | 20.75 | 65.98 |

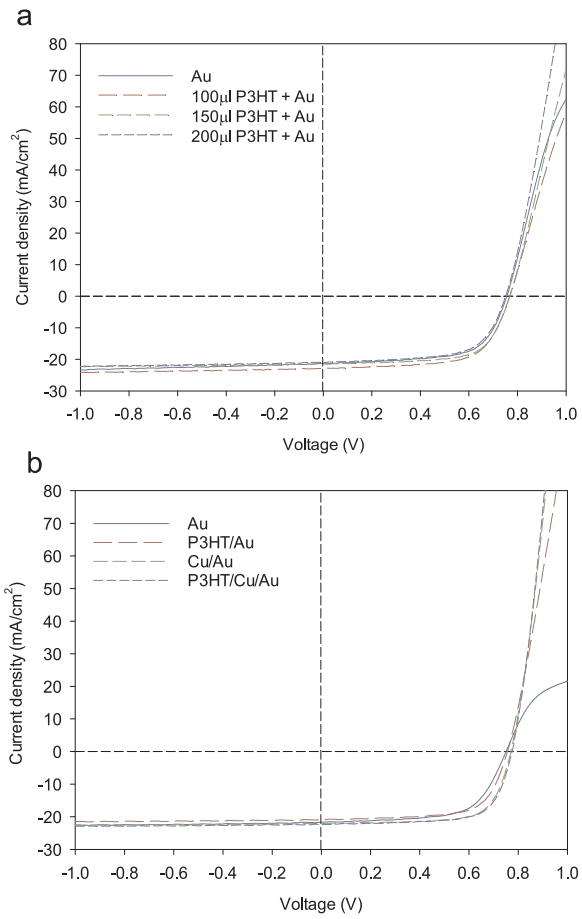


**Fig. 4.** a) *JV* curves for highest efficiency contacts for an Au contacted control and cells coated using 100, 150 and 200 µl of P3HT solution, b) *JV* curves comparing the highest efficiency devices having Au, Cu/Au, P3HT/Au and P3HT/Cu/Au contact structures (only the plain Au shows rollover).

contacts.

Table 2 gives the peak and average performance parameters respectively for the four compared contact structures: i) Au, ii) P3HT/Au, iii) Cu/Au and iv) P3HT/Cu/Au. *JV* curves for the highest efficiency contact from each cell are given in Fig. 4b along with associated EQE analysis in Fig. 5.

As with the previous *JV* data the P3HT/Au contacts show an increase in the peak performance from 10.49% to 11.29% compared to Au contacting through an improvement in both the $V_{OC}$ and *FF*. From the *JV* curves it is again apparent that the device rollover has been eliminated by the inclusion of the P3HT layer. As one may expect, use of a Cu/Au back contact layer yields a further improvement to 12.30% most probably through additional Cu-doping not achieved by the P3HT layer and to an extent independent of the back contact barrier. By introducing the P3HT layer prior to copper deposition to form a P3HT/Cu/Au contact structure, there is negligible loss in the peak performance compared to Cu/Au contacting at 12.26%. Dark *JV* measurements imply there is some additional series resistance component in the P3HT/Cu/Au contact compared to Cu/Au contacting (there is a decreased gradient at forward bias) but this does not appear to be a problem for light *JV* measurements. EQE analysis shows little change at shorter wavelengths but there are variations at longer wavelengths as seen in Fig. 5b. The P3HT/Au, Cu/Au and P3HT/Cu/Au contacted cells show improved deep collection compare to the Au contact via a higher EQE response at longer wavelengths. The P3HT and P3HT/Cu/Au contacted cells however show a small amount of additional collection at wavelengths > 850 nm (Fig. 5b). The exact cause of this behaviour is unclear at present. It may be in someway related to the back contact annealing step, of which the Au contact has not been subjected but the other have. What is also clear is that there is some additional effect due to the P3HT generating the small additional response above 850 nm. This may be related to simple interface reflection or possibly recombination at the back surface has been reduced by its presence but further work is required to examine this.

Assessment of the barrier heights of the contacts was made by current-voltage-temperature (*JVT*) analysis. *JV* curves were recorded in the dark in the temperature range $T$ = 200–300 K. From each curve an $R_S$ values was determined using the method of Batzner et al. [1], wherein the $R_s(T)$ behaviour may be separated into Ohmic, a negative

**Table 2**
Performance data for cells having contacts with added Cu and controls (see text). In each case the data is for nine unscribed electrodes having an area of 0.24 $cm^2$ each. For the contacts with P3HT, they were prepared by spinning 100 µl of solution.

| Contact | | Efficiency (%) | $V_{OC}$ (V) | $J_{SC}$ (mA/$cm^2$) | *FF* (%) |
|---|---|---|---|---|---|
| **Au** | *Ave* | 9.04 ± 2.41 | 0.704 ± 0.111 | 20.61 ± 0.72 | 60.50 ± 9.73 |
| | *Peak* | 10.49 | 0.75 | 21.66 | 64.91 |
| **P3HT/Au** | *Ave* | 10.17 ± 0.91 | 0.751 ± 0.020 | 20.77 ± 0.55 | 65.07 ± 3.06 |
| | *Peak* | 11.29 | 0.77 | 21.82 | 68.66 |
| **Cu/Au** | *Ave* | 4.50 ± 5.51 | 0.360 ± 0.323 | 17.91 ± 5.65 | 40.77 ± 21.55 |
| | *Peak* | 12.30 | 0.78 | 22.54 | 69.95 |
| **P3HT/Cu/Au** | *Ave* | 10.00 ± 2.24 | 0.7311 ± 0.058 | 21.10 ± 0.87 | 63.89 ± 8.02 |
| | *Peak* | 12.26 | 0.78 | 22.37 | 70.80 |

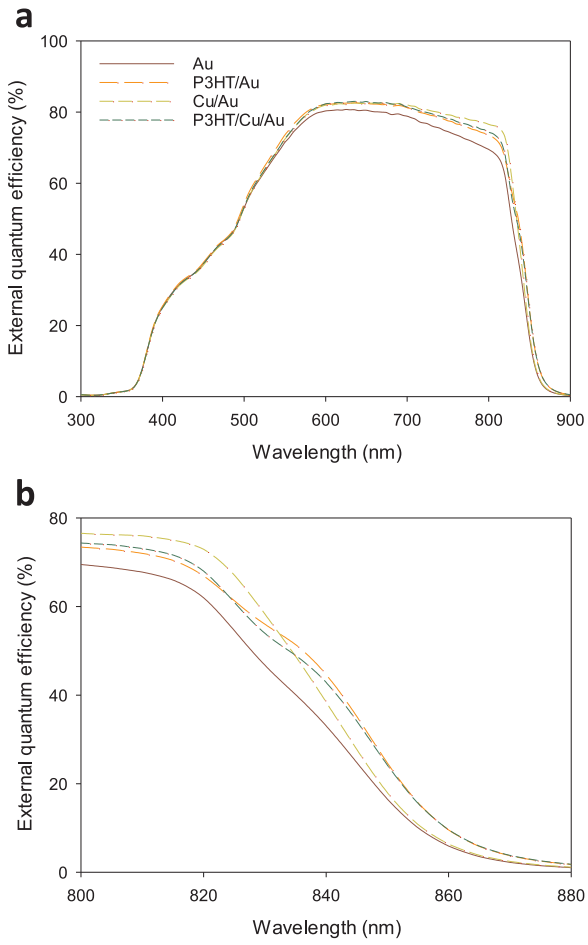


**Fig. 5.** EQE curves for highest efficiency devices having Au, Cu/Au, P3HT/Au and P3HT/Cu/Au contact structures over a) 300–900 nm range and b) focussing on the 800–880 nm range.

temperature coefficient and an exponential part, the latter relating to thermionic emission over the back contact barrier. The expression for $R_S$ is given in Eq. (1) as;

$$R_s = R_{\Omega 0} + \frac{\partial R_{\Omega 0}}{\partial T} T + \frac{C}{T^2} \exp\left(\frac{\varphi_b}{kT}\right) \quad (1)$$

where $R_{\Omega 0}$ is the Ohmic resistance, $\frac{\partial R_{\Omega 0}}{\partial T}$ is its temperature coefficient, $C$ is a fitting parameter, k is the Boltzmann constant and $\varnothing_b$ is the back contact barrier height. The barrier height can therefore be determined from a fit to the exponential behaviour of the $R_S(T)$ curve. Fig. 6 shows

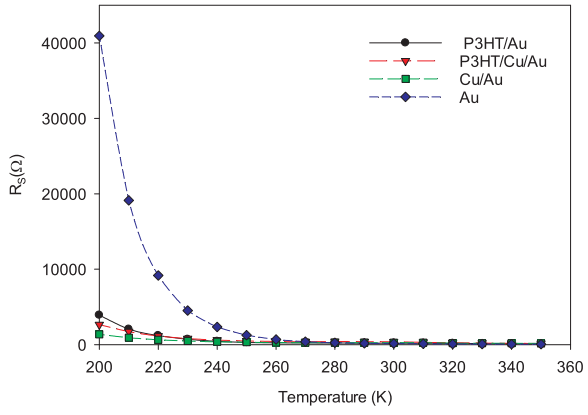


**Fig. 6.** $R_S$ vs $T$ for highest efficiency devices having Au, Cu/Au, P3HT/Au and P3HT/Cu/Au contact structures.

example $R_s$ vs $T$ data for devices contacted with either Au, P3HT/Au, Cu/Au or P3HT/Cu/Au.

It is striking that the plain Au contact has both the highest resistances and the strongest exponential character while all of the other contact types shown in Fig. 6 form a group having lower resistance and weaker temperature dependence. Clearly, both P3HT on its own, and any contact containing Cu is able to reduce the apparent electrical barrier to the CdTe.

This is borne out in the barrier heights extracted by fitting: plain Au contacts have values in the range of 0.39–0.42 eV, whilst for Cu/Au and P3HT/Cu/Au contacts this value was reduced to 0.21–0.22 eV. This reduction is consistent with the reduction in rollover shown in Fig. 4b. P3HT/Au contacts yielded barriers in the range 0.29–0.33 eV. On a practical point we note that for this particular sample type, the $R_s$ vs $T$ plots had a tendency to be linear making fitting of the exponential component unreliable. These values are therefore only typical of a subset of the P3HT/Au samples for which the fitting was feasible. It is not clear whether this abnormal behaviour is due to physical changes to the P3HT in the cryostat or else to a genuine difference in the current transport over the contact interface. Overall the barrier heights that were measured were comparable to the range expected from comparison with those in the literature and are consistent with the observations of rollover in the *JV* curves.

A key point to note from this device series, rather than the peak performance value itself, is the improvement in the *average* device performance measured when P3HT is included (either with or without Cu). Due to the large CdTe grain size generated by the CSS deposition process [33,34], coverage may be incomplete, and pinholes in the film are common. The impact of these pinholes can vary in severity from degradation of performance through shunting (causing reduced *FF* and $V_{OC}$ [16]), to complete cell breakdown. Typically for our deposition process we anticipate a number of the 0.25 $cm^2$ contacts on a given cell plate will be compromised by pinholes in the CdTe film. Whilst we see that this is a problem for Au contacted devices, it is further exacerbated by the inclusion of copper, presumably due to it's having a direct pathway into the CdS layer. For this sample set the glass cleaning was purposefully minimised (no ozone or plasma cleaning of the $SnO_2$-coated glass) to increase the pinhole content.

A preliminary evaluation of the effect of the CdTe non-uniformity ('pinholes') was made by examining the number of short circuited contacts and the spread of performances for each group of nine contact pads on any given device. The following observations for the devices reported in Table 2 were typical for devices prepared from the same CdTe starting material (i.e. having the same density of pinholes):

a) Plain Au-contacted device: one contact pad from nine had a pinhole, reducing its performance to 2.7% ($V_{OC}$ = 0.41 V; *FF* = 34.8%).
b) P3HT/Au-contacted device: two or three pads from nine with visible pinholes. Lowest performance remained relatively high at 8.32% ($V_{OC}$ = 0.71 V; *FF* = 58.9%).
c) Cu/Au-contacted device: two completely shunted contacts having efficiency < 0.1% and $V_{OC}$ < 0.1 V; two further contacts with efficiency below 2%. i.e. four poor performing contact pads from nine.
d) P3HT/Cu/Au-contacted device: two or three contact pads with pinholes in a total of nine. Lowest performance 6.45% ($V_{OC}$ = 0.71 V; *FF* = 58.9%).

These results were confirmed on other sample sets and indicate that P3HT in all cases acts to reduce the deleterious effect of pinholes on device performance. This motivated the fuller statistical treatment of uniformity and pinhole effects that follows in Section 2.3.

We now report the effects of the contacts on high performance cells rather than those above. The previous cell results were developed using our standard cell platform which incorporates a comparatively thick CdS layer (~ 160 nm). This provides a highly consistent baseline cell which is suitable for self-consistent investigations, but which has a low

**Table 3**
Peak and average performance parameters for P3HT/Cu/Au and Cu/Au contacts for higher $V_{OC}$ cell devices including a CdS:O layer.

| Contact | | Efficiency (%) | $V_{OC}$ (V) | $J_{SC}$ (mA/cm$^2$) | FF (%) |
|---|---|---|---|---|---|
| **Cu/Au** | *Ave* | 12.06 ± 4.57 | 0.737 ± 0.272 | 22.65 ± 6.30 | 61.26 ± 15.26 |
| | *Peak* | 14.72 | 0.837 | 25.04 | 70.24 |
| ***P$_3$HT/Cu//Au*** | *Ave* | 14.25 ± 0.47 | 0.841 ± 0.009 | 25.49 ± 0.73 | 66.49 ± 2.86 |
| | *Peak* | 14.66 | 0.848 | 25.22 | 68.55 |

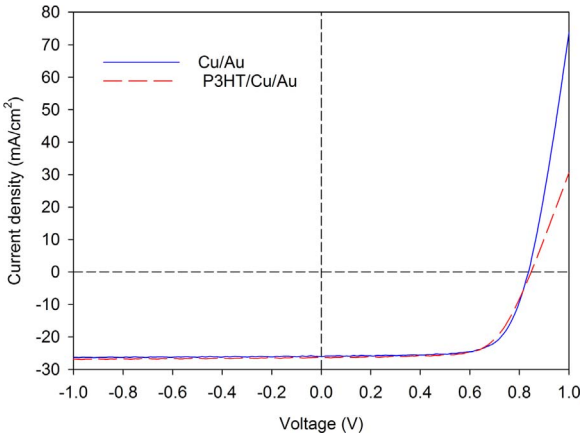


**Fig. 7.** JV curves for P3HT/Cu/Au and Cu/Au contacts for higher $V_{OC}$ cell platform including CdS:O layer.

cell efficiency. We also wished to compare the P3HT-containing contacts on higher $V_{OC}$ devices to assess whether performance can be maintained or improved by the inclusion of the organic layer. The highest efficiency devices produced at Liverpool incorporate a nanostructured CdS:O window layer [25] which has a higher bandgap due to quantum confinement effects [35]. Cells which incorporate these layers rather than standard CdS typically have a significantly higher $V_{OC}$. We do not use these layers as standard for process optimisation due to problems associated with reproducibility of the deposition process and formation of various oxide phases [36]. Nevertheless, these window layers are capable of generating high performance so are useful as single run test beds for the contact structures. Table 3 gives *JV* performance parameters associated *JV* curves for highest efficiency contacts area show in Fig. 7 for such devices having either Cu/Au or P3HT/Cu/Au contacts (processes as described before). Both samples are from the same deposition run so there are no concerns about process variation due to the CdS:O. The relative peak efficiency for these devices was near identical at 14.72% for the Cu/Au contacts and 14.66% for a P3HT/Cu/Au cell. *JV* curves indicate that the addition of the P3HT has led to a slight increase in the series resistance. This has marginally reduced the fill factor from 70.2% to 68.6% but the $V_{OC}$ has conversely increased from 837 mV to 848 mV. The $J_{sc}$ shows little variation. As with previous samples though the average efficiency across 9 contact pads for these cells is greatly improved through then inclusion of P3HT, being 12.06 ± 4.56% for the Cu/Au contact and 14.24 ± 0.46% for the P3HT/Cu/Au contact. In essence the inclusion of P3HT has not adversely impacted upon the peak device performance but has yielded improved uniformity of performance. This improvement in uniformity is better quantified in the following section.

### 3.3. Pinhole blocking behaviour

Since pinholing is by its nature an uncontrolled phenomenon it can be problematic to study. we have adopted two approaches to making systematic studies of pinhole healing using P3HT contacts:

a) firstly we have grown CdTe samples which would purposefully contain significant pinholing. These comprised CSS-grown CdTe having a thickness gradient, with pinholing being more prevalent for the thinner parts (this also had the advantage of generating thickness-dependent device data).
b) secondly we used a meta-analysis of performance data from the several hundred contacts made during the course of this study.

#### 3.3.1. Cells on graded CdTe

The CdTe absorbers were grown on 50 × 50 mm$^2$ substrates and had an intentional thickness variation from 0.7 to 1.9 μm. For CSS CdTe layers, owing to the large grain size, films of < 1.5 μm thickness tend to produce a significant amount of shunting. The plate was $MgCl_2$ treated and then divided into two 25 × 50 mm$^2$ contact plates. One of these plates was contacted with a Cu/Au stack whilst the second was contacted with a P3HT/Cu/Au stack structure. Each of the two plates contained 18 individual contacts which were measured via *JV* analysis as well as having the film thickness of the CdTe at the contact position analysed via a surface profiler measurement following scribing. Table 4 gives the average and peak performance parameters for the two sample plates, whilst individual contact performance is plotted as a function of the CdTe absorber thickness in Fig. 8a–d for both contact structures.

The improvement for these devices generated by the addition of P3HT is clear, both the average and peak performance is improved, with there being no contact performing < 5% for the P3HT containing device. In contrast the Cu/Au contacted plate shows a number of "dead" contacts, or else contacts where shunting due to pinholes was dominant. The losses are particularly apparent in the low *FF* and $V_{oc}$ values for the Cu/Au devices.

A further feature of the data in Fig. 8a–d is that for the cells with P3HT contacts, the data follows a clear systematic trend. For the thinner devices there is a drop-off in efficiency (below 2 μm) that has been accounted for as optical transmission loss by both modelling and experiment [37]. However, this trend is not visible for the Cu/Au-contacted devices in the same thickness range: instead the plot is dominated by scatter caused by shunting. This is a demonstration of the

**Table 4**
Performance data for sets of 18 contact pads deposited on CdTe grown under conditions to encourage pinholes. The CdTe was CSS-grown and had an intentional thickness gradient (0.7–1.9 μm over 50 mm). Peak and average performance parameters are shown here, while the thickness dependent data itself is shown in Fig. 6. Use of P3HT in the contacts increases the average performance by maintaining a high *Voc*.

| Contact | | Efficiency (%) | $V_{OC}$ (V) | $J_{SC}$ (mA/cm$^2$) | *FF* (%) |
|---|---|---|---|---|---|
| **Cu/Au** | *Ave* | 3.70 ± 3.60 | 0.399 ± 0.263 | 17.60 ± 4.52 | 37.91 ± 15.96 |
| | *Peak* | 10.25 | 0.750 | 21.27 | 67.29 |
| **P$_3$HT/Cu/Au** | *Ave* | 8.33 ± 1.54 | 0.714 ± 0.054 | 19.64 ± 1.05 | 58.69 ± 4.79 |
| | *Peak* | 10.59 | 0.780 | 20.97 | 65.13 |

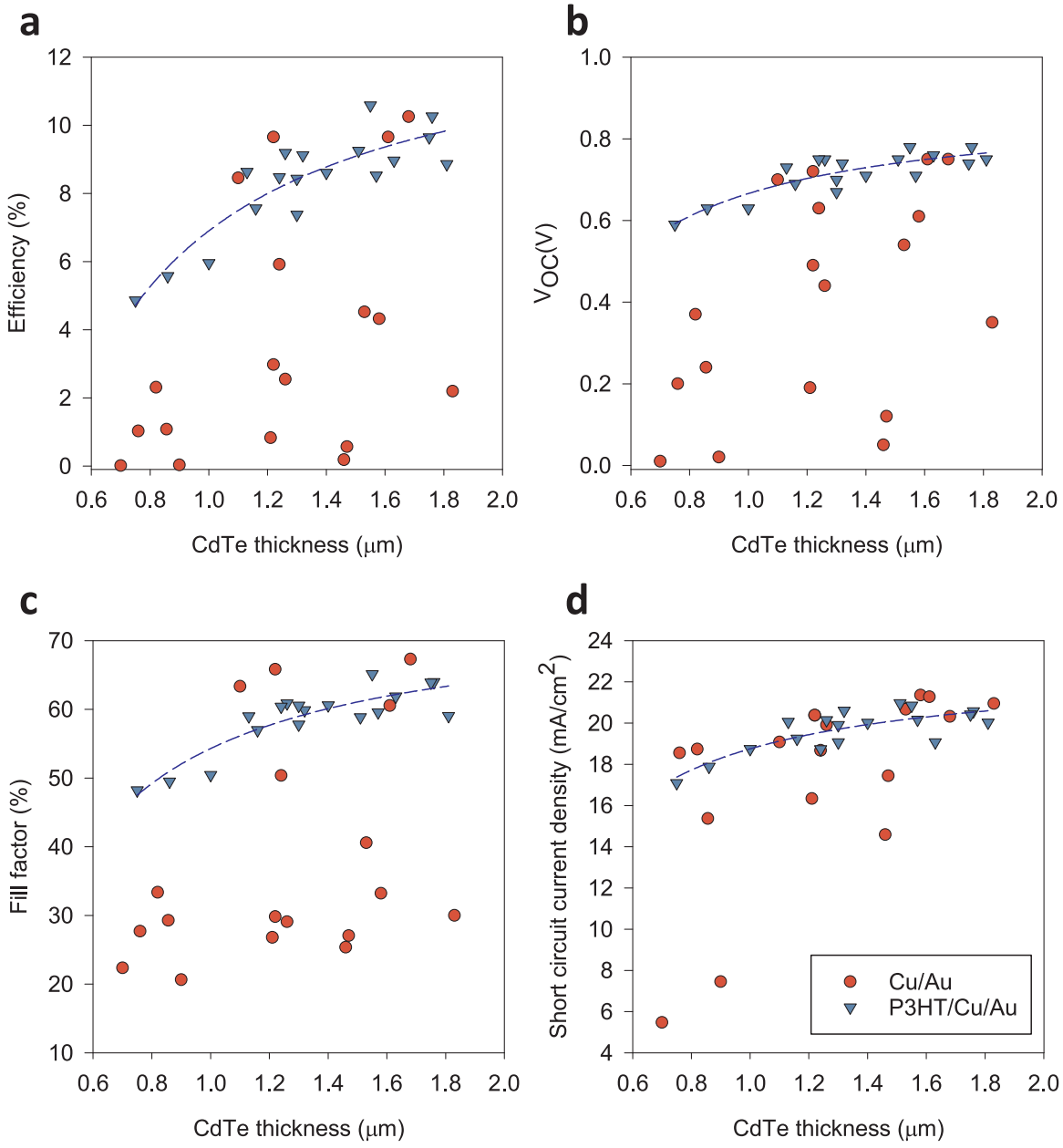


**Fig. 8.** a)–d) Cell performance parameters as a function of CdTe thickness for cells contacted with Cu/Au and with P3HT/Cu/Au.

benefit to uniformity of including P3HT into the contact structure.

### 3.3.2. *Meta-analysis of cell performance*

The performance parameters of the 600 individual device contacts fabricated for this study allowed the effects of P3HT to be evaluated over a large sample set. This was done to determine the overall reliability of the P3HT process and to evaluate a "typical' level of improvement by employing the process. Of the four working parameters we chose *Voc* as it is a simple indicator of overall junction quality as it is generally considered to be sensitive to shunting effects (other performance parameters display a similar trend however).

Fig. 9a shows all $V_{OC}$ values determined for contact pads measured as part of this work separated into 429 P3HT contacted and 171 non-P3HT types. The plot axis is simply the chronological sample number for each series. In order to consider the largest data seta available we included *all* the devices made during the study without selection, and this included those with and without Cu, and those formed using different thicknesses of P3HT for example. While Fig. 9a shows a clear line of higher performance at around 800 mV, many devices fall short of this and contribute to the scatter of points at lower $V_{oc}$ that is attributed to shunting (as confirmed from the data in Fig. 8a–d). The initial impression that P3HT contacts have fewer failures was explored by the $V_{oc}$ threshold plot shown in Fig. 9b. Here we exploit the idea that a failed device can be characterised as having a $V_{oc}$ below an arbitrary threshold level. The plot shows the percentage of 'failed' devices vs this $V_{oc}$ threshold for both the P3HT- and non-P3HT contacted devices. The failure gradient for P3HT contacted devices is considerably lower than that for those with metal contacts. This indicates that the failure fraction is not only lower for P3HT contacts, but that this is true whatever voltage threshold is chosen. For example, we consider a threshold *Voc* value of 600 mV to be informative as this reflects a the typical peak $V_{OC}$ value one can realistically expect from an untreated (i.e. not chloride treated) cell [38]. Any $V_{OC}$ which falls below this level has therefore clearly been compromised by pinholes to some extent. Of the 429 P3HT contacted cells measured there were 34 contacts with a $V_{OC} < 600$ mV, a contact failure rate of ~ 7.9%. In the same period 171 contacts were

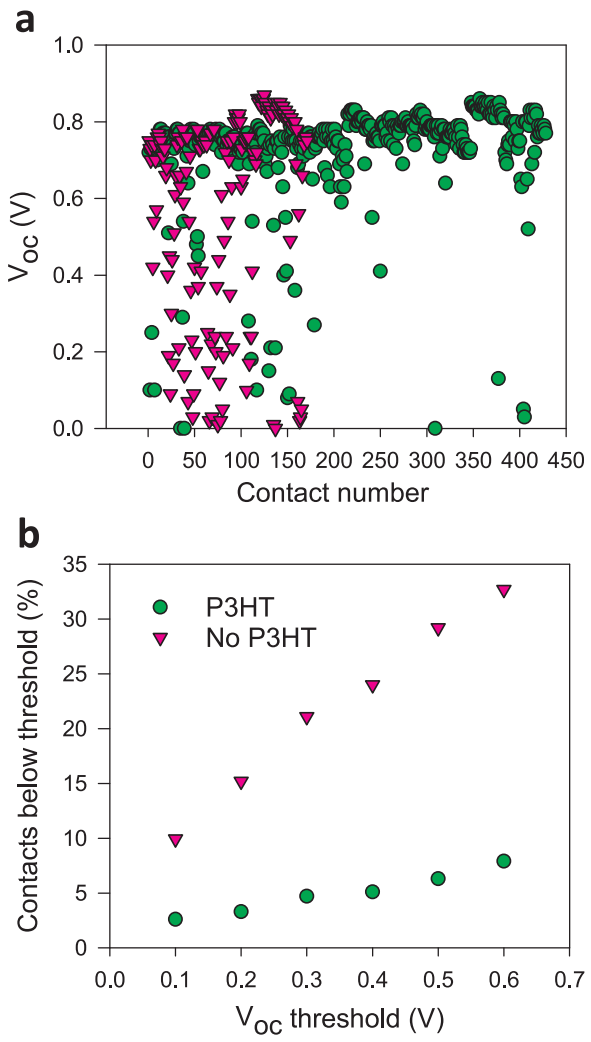


**Fig. 9.** a) Compendium of all $V_{OC}$ data for the ~ 600 devices measured in this study displayed by their chronological serial number. The plot compares the performance of contacts with P3HT (429 – both with and without Cu – green circles) and for Au metallic contacts (171 – both with and without Cu – purple triangles), b) percentage of contacts having $V_{OC}$ below a variable threshold vs that threshold – this plot demonstrates that contacts incorporating P3HT are less susceptible to $V_{OC}$ losses from pinholing compared to metal-only contacts. (For interpretation of the references to color in this figure legend, the reader is referred to the web version of this article.)

measured for devices with either Au or Cu/Au contacts. Of these, 56 contacts had $V_{OC}$ < 600 mV, a failure rate of ~ 32.7%. Since the plots in Fig. 9b are essentially linear over the considered range, selection of a different voltage threshold criterion give the same ratio of failures for the two classes of contact i.e. for a threshold of 100 mV the failure rate is 9.9% for metal contacts and 2.6% for those with P3HT. Overall the data support the conclusion that P3HT acts to increase the uniformity of the solar cell performance by reducing the deleterious impact of pinholes.

### 3.4. Contact stability

Organic and perovskite PV devices are often blighted by problems of both short and longer term instability often due to sensitivity to air and/or moisture [39]. It is therefore a natural concern that, being an organic molecule, P3HT may suffer from the same problem when used as a contact and that there may be degradation, although there appears to be little evidence to this effect. Nevertheless, in order to test this two devices were compared. The first cell had a simple Au contact whilst the second had a P3HT/Au contact, with all other fabrication and

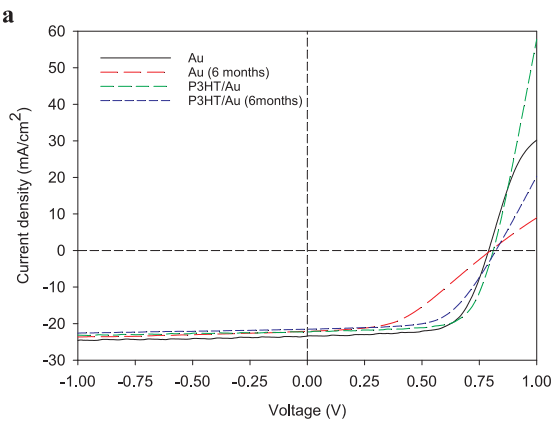


b

| Contact | Efficiency variation (%) | $V_{OC}$ (%) | $J_{SC}$ (%) | FF (%) |
|---|---|---|---|---|
| *Au* | -27.2 ± 8.5 | 1.7 ± 1.2 | -6.1 ± 5.4 | -23.6 ± 8.4 |
| *P3HT/Au* | -8.9 ± 12.0 | 5.0 ± 9.5 | -4.4 ± 1.8 | -9.4 ± 4.8 |

**Fig. 10.** a) *JV* curves for the highest efficiency contacts for Au and P3HT/Au contacted cells before and after a 6 month ambient aging process, b) change in average performance parameters after 6 months.

processing steps were identical. Copper was not included in the back contact as this is already known to lead to performance degradation in CdTe cells and would potentially dominate the results. Both cells were measured via *JV* and then stored under ambient lab conditions for 6 months before being re-measured. *JV* curves for the highest efficiency contact from each device before and after aging are given in Fig. 10a along with the relative percentage shift in the extracted average performance parameters being given in Fig. 10b. From these results it was established that rather than enhance the degradation the P3HT layer has actually served to lessen the degradation of the gold contact. Whereas the Au contact degraded by a relative 27.2% in efficiency the P3HT/Au stack degraded by only 8.9%. In both cases, although there is some $J_{sc}$ loss, the losses primarily arise from *FF* decreases as a result of higher series resistance, which can be seen in the *JV* curves. This is presumable due to oxides such as CdO [40], $CdTeO_3$ [41] or $TeO_2$ [42], forming beneath the Au contact as a result of water vapour penetration though the Au. Therefore it may be presumed that the P3HT blocks the ingress of water vapour and prevents oxidation of the underlying semiconductor.

## 4. Conclusion

This work presented a comparison of P3HT-containing contacts with Au metallisations and their effect on the performance and uniformity of performance of CdTe solar cells. Spin coating was sufficient to generate conformal coatings of P3HT on rough CdTe surfaces where it acted to fill in fissures at grain boundaries. An XPS study of the ionisation potentials of cleaned P3HT and CdTe surfaces generated data that was used to predict the band line ups of the interface between the two - it was found that a) no barrier to hole emission from the CdTe and b) an electron reflecting barrier were expected. In practice, a reduced hole barrier of 0.29–0.33 eV was measured for P3HT/Au, this being lower than for plain Au. Inclusion of Cu-doping to contacts further reduced the barrier height with or without P3HT. Future analysis via secondary ion mass spectrometry (SIMS) is required to confirm the apparent transparency of the P3HT to copper diffusion. The principal benefit of P3HT contacting was shown to be in increasing the uniformity of performance, both over large numbers of devices, and within single device plates. Samples were grown to demonstrate this and the conclusion was also supported by meta-analysis of *Voc* data from 600 devices. Graphs of 'failure' vs *Voc* threshold were also used to corroborate the finding that P3HT acts to 'heal' pinholes. Use of P3HT contacts was also shown

to be valuable in allowing reliable data trends to be identified by eliminating the scatter from shunting. P3HT contacts imparted greater stability to CdTe solar cells than was observed for Au contacts. Overall, P3HT has been demonstrated to increase the uniformity and run to run repeatability of the performance of laboratory CdTe solar cells. Further work may include doping the P3HT (in order to further reduce its series resistance or to manipulate the band line ups), with for example lithium bis(trifluoromethanesulfonyl)imide, and the exploration of other organic materials for use as solar cell contacts.

## Data availability

The data which supports the findings of this work is available at https://zenodo.org/deposit/802852 or from the author.

## Acknowledgements

This work was funded by the UK Engineering and Physical Sciences Research Council Grant nos. EP/J017361/1 and EP/N014057/1.

## References

[1] D.L. Batzner, M.E. Oszan, D. Bonnet, K. Bucher, Device analysis methods for physical cell parameters of CdTe/Cds solar cells, Thin Solid Films 361 (2000) 288–292.
[2] A.R. Davies, J.R. Sites, Effects of non-uniformity on rollover phenomena in CdS/CdTe solar cells, in: Proceedings of the i2008 33rd Ieee Photovoltaic Specialists Conference, San Diego, 2008, pp. 242–244.
[3] S.H. Demtsu, J.R. Sites, Effect of back-contact barrier on thin-film CdTe solar cells, Thin Solid Films 510 (2006) 320–324.
[4] J. Zhou, X. Wu, A. Duda, G. Teeter, S.H. Demtsu, The formation of different phases of CuxTe and their effects on CdTe/CdS solar cells, Thin Solid Films 515 (2007) 7364–7369.
[5] M. Nardone, D.S. Albin, Degradation of CdTe solar cells: simulation and experiment, IEEE J. Photovolt. 5 (2015) 962–967.
[6] T.A. Gessert, W.K. Metzger, P. Dippo, S.E. Asher, R.G. Dhere, M.R. Young, Dependence of carrier lifetime on Cu-contacting temperature and ZnTe:Cu thickness in CdS/CdTe thin film solar cells, Thin Solid Films 517 (2009) 2370–2373.
[7] N. Romeo, A. Bosio, R. Tedeschi, V. Canevari, Back contacts to CSSCdS/CdTe solar cells and stability of performances, Thin Solid Films 361 (2000) 327–329.
[8] K.P. Bhandari, P. Koirala, N.R. Paudel, R.R. Khanal, A.B. Phillips, Y.F. Yan, R.W. Collins, M.J. Heben, R.J. Ellingson, Iron pyrite nanocrystal film serves as a copper-free back contact for polycrystalline CdTe thin film solar cells, Sol. Energy Mater. Sol. Cells 140 (2015) 108–114.
[9] I. Irfan, H. Lin, W. Xia, H.N. Wu, C.W. Tang, Y. Gao, The effect of MoOx inter-layer on thin film CdTe/CdS solar cell, Sol. Energy Mater. Sol. Cells 105 (2012) 86–89.
[10] H. Lin, Irfan, W. Xia, H.N. Wu, Y. Gao, C.W. Tang, MoOx back contact for CdS/CdTe thin film solar cells: preparation, device characteristics, and stability, Sol. Energy Mater. Sol. Cells 99 (2012) 349–355.
[11] H. Lin, W. Xia, H.N. Wu, C.W. Tang, CdS/CdTe solar cells with MoOx as back contact buffers, Appl. Phys. Lett. 97 (2010).
[12] W. Wang, N.R. Paudel, Y. Yan, F. Duarte, M. Mount, PEDOT, PSS as back contact for CdTe solar cells and the effect of PEDOT:PSS conductivity on device performance, J. Mater. Sci.-Mater. Electron. 27 (2016) 1057–1061.
[13] S. Dayal, H.Z. Zhong, N. Kopidakis, G.D. Scholes, G. Rumbles, Improved power conversion efficiency for bulk heterojunction solar cells incorporating CdTe-CdSe nanoheterostructure acceptors and a conjugated polymer donor, J. Photonics Energy 5 (2015) 9.
[14] W.-J. Huang, S.A. De Valle, J.B.K. Kana, K. Simmons-Potter, B.G. Potter Jr., Integration of CdTe-ZnO nanocomposite thin films into photovoltaic devices, Sol. Energy Mater. Sol. Cells 137 (2015) 86–92.
[15] S.Y. Yao, Z.L. Chen, F.H. Li, B. Xu, J.X. Song, L.L. Yan, G. Jin, S.P. Wen, C. Wang, B. Yang, W.J. Tian, High-efficiency aqueous-solution-processed hybrid solar cells based on P3HT dots and CdTe nanocrystals, ACS Appl. Mater. Interfaces 7 (2015) 7146–7152.
[16] N.E. Gorji, Degradation sources of CdTe thin film PV:CdCl2 residue and shunting pinholes, Appl. Phys. A-Mater. Sci. Process. 116 (2014) 1347–1352.
[17] G.T. Koishiyev, J. Sites, Effect of shunts on thin-film CdTe module performance, in: Proceedings of the Materials Research Society Symposium Proceedings, vol. 1165, 2009, pp. M05–M22.
[18] G.T. Koishiyev, J.R. Sites, Ieee, effect of weak diodes on the performance of CdTe thin-film modules, in: Proceedings of the 34th Ieee Photovoltaic Specialists Conference, Philladelphia, 2009, pp. 79–82.
[19] V.G. Karpov, A.D. Compaan, D. Shvydka, Effects of nonuniformity in thin-film photovoltaics, Appl. Phys. Lett. 80 (2002) 4256–4258.
[20] V.G. Karpov, A.D. Compaan, D. Shvydka, Random diode arrays and mesoscale physics of large-area semiconductor devices, Phys. Rev. B 69 (2004) 12.
[21] M.M. Tessema, D.M. Giolando, Pinhole treatment of a CdTe photovoltaic device by electrochemical polymerization technique, Sol. Energy Mater. Sol. Cells 107 (2012) 9–12.
[22] Y. Roussillon, D.M. Giolando, D. Shvydka, A.D. Compaan, V.G. Karpov, Blocking thin-film nonuniformities: photovoltaic self-healing, Appl. Phys. Lett. 84 (2004) 616–618.
[23] D.K. Koll, A.H. Taha, D.M. Giolando, Photochemical "Self-healing" pyrrole based treatment of CdS/CdTe photovoltaics, Sol. Energy Mater. Sol. Cells 95 (2011) 1716–1719.
[24] J.D. Major, Y.Y. Proskuryakov, K. Durose, Impact of CdTe surface composition on doping and device performance in close space sublimation deposited CdTe solar cells, Progress. Photovolt. 21 (2013) 436–443.
[25] J.D. Major, R.E. Treharne, L.J. Phillips, K. Durose, A low-cost non-toxic post-growth activation step for CdTe solar cells, Nature 511 (2014) 334–337.
[26] T.J. Whittles, L.A. Burton, J.M. Skelton, A. Walsh, T.D. Veal, V.R. Dhanak, Band alignments, valence bands, and core levels in the Tin sulfides SnS, SnS2, and Sn2S3: experiment and theory, Chem. Mater. 28 (2016) 3718–3726.
[27] J.D. Major, L. Bowen, K. Durose, Focussed ion beam and field emission gun-scanning electron microscopy for the investigation of voiding and interface phenomena in thin-film solar cells, Progress. Photovolt. 20 (2012) 892–898.
[28] C.G. Van de Walle, Universal alignment of hydrogen levels in semiconductors and insulators, Phys. B-Condens. Matter 376 (2006) 1–6.
[29] Y.H. Li, A. Walsh, S.Y. Chen, W.J. Yin, J.H. Yang, J.B. Li, J.L.F. Da Silva, X.G. Gong, S.H. Wei, Revised ab initio natural band offsets of all group IV, II-VI, and III-V semiconductors, Appl. Phys. Lett. 94 (2009).
[30] G. Teeter, X-ray and ultraviolet photoelectron spectroscopy measurements of Cu-doped CdTe(111)-B: observation of temperature-reversible Cu(x)Te precipitation and effect on ionization potential, J. Appl. Phys. 102 (2007).
[31] K.-J. Hsiao, J.R. Sites, Ieee, electron reflector startegy for CdTe solar cells, in: Proceedings of the 34th Ieee Photovoltaic Specialists Conference, Philladelphia, 2009, pp. 1352–1356.
[32] K.-J. Hsiao, J.R. Sites, Electron reflector to enhance photovoltaic efficiency: application to thin-film CdTe solar cells, Progress. Photovolt. 20 (2012) 486–489.
[33] J.D. Major, Grain boundaries in CdTe thin film solar cells: a review, Semicond. Sci. Technol. 31 (2016).
[34] J.D. Major, Y.Y. Proskuryakov, K. Durose, G. Zoppi, I. Forbes, Control of grain size in sublimation-grown CdTe, and the improvement in performance of devices with systematically increased grain size, Sol. Energy Mater. Sol. Cells 94 (2010) 1107–1112.
[35] X. Wu, Y. Yan, R.G. Dhere, Y. Zhang, J. Zhou, C. Perkins, B. To, Nanostructured CdS, O film: preparation, properties, and application, in: Proceedings of the 11th International Conference on Ii-Vi Compounds (Ii-Vi 2003), Proceedings, 2004, pp. 1062–1066.
[36] D.A. Duncan, J.M. Kephart, K. Horsley, M. Blum, M. Mezher, L. Weinhardt, M. Haming, R.G. Wilks, T. Hofmann, W.L. Yang, M. Bar, W.S. Sampath, C. Heske, Characterization of Sulfur bonding in CdS:O buffer layers for CdTe-based thin-film solar cells, ACS Appl. Mater. Interfaces 7 (2015) 16382–16386.
[37] M.M. Nowell, M.A. Scarpulla, N.R. Paudel, K.A. Wieland, A.D. Compaan, X.X. Liu, Characterization of sputtered CdTe thin films with electron Backscatter diffraction and correlation with device performance, Microsc. Microanal. 21 (2015) 927–935.
[38] J.D. Major, M. Al Turkestani, L. Bowen, M. Brossard, C. Li, P. Lagoudakis, S.J. Pennycook, L.J. Phillips, R.E. Treharne, K. Durose, In-depth analysis of chloride treatments for thin-film CdTe solar cells, Nat. Commun. 7 (2016).
[39] A.M.A. Leguy, Y. Hu, M. Campoy-Quiles, M.I. Alonso, O.J. Weber, P. Azarhoosh, M. van Schilfgaarde, M.T. Weller, T. Bein, J. Nelson, P. Docampo, P.R.F. Barnes, Reversible hydration of $CH_3NH_3PbI_3$ in films, single crystals, and solar cells, Chem. Mater. 27 (2015) 3397–3407.
[40] J. Fritsche, S. Gunst, E. Golusda, M.C. Lejard, A. Thissen, T. Mayer, A. Klein, R. Wendt, R. Gegenwart, D. Bonnet, W. Jaegermann, Surface analysis of CdTe thin film solar cells, Thin Solid Films 387 (2001) 161–164.
[41] B.E. McCandless, S.S. Hegedus, R.W. Birkmire, D. Cunningham, Correlation of surface phases with electrical behavior in thin-film CdTe devices, Thin Solid Films 431 (2003) 249–256.
[42] D.W. Niles, D. Waters, D. Rose, Chemical reactivity of CdCl2 wet-deposited on CdTe films studied by X-ray photoelectron spectroscopy, Appl. Surf. Sci. 136 (1998) 221–229.